New isospin-breaking "USD" Hamiltonians for the *sd* shell

A. Magilligan and B. A. Brown
Department of Physics and Astronomy and National Superconducting Cyclotron Laboratory, and Michigan State University, East Lansing, Michigan 48824, USA

(Received 17 December 2019; accepted 22 May 2020; published 15 June 2020)

Two new USD-type Hamiltonians, USDC and USDI, have been developed that directly incorporate Coulomb and other isospin-breaking interactions. Starting from *ab initio* interactions, linear combinations of two-body matrix elements were constrained by experimental energy levels in *sd*-shell nuclei. With this method, binding energies and excitation energies of proton-rich nuclei in the shell can be added to the data set used in the fit. USDC is based on the same renormalized G matrix used in the derivation of previous USD-type Hamiltonians, while USDI is derived from in-medium similarity renormalization group (IMSRG) interactions. Both contain an analytic Coulomb interaction with Miller-Spencer short-range correlations and an effective isotensor interaction. Also presented are modifications to these interactions, USDCm and USDIm, that have had the Coulomb interaction constrained to better reproduce the experimental b coefficients of the isobaric mass multiplet equation. These Hamiltonians are used to provide new predictions for the proton-dripline and to examine isospin-level mixing and other properties of *sd*-shell nuclei. An empirical expression for the Thomas-Ehrman shift in loosely bound and unbound proton-rich states is presented, and several such states are examined.

DOI: 10.1103/PhysRevC.101.064312

I. INTRODUCTION

The universal *sd* shell (USD) Hamiltonian [1,2] has provided realistic *sd*-shell ($0d_{5/2}$, $0d_{3/2}$, $1s_{1/2}$) wave functions for use in nuclear structure models, nuclear spectroscopy, and nuclear astrophysics since its development thirty-five years ago. Its successors USDA and USDB [3,4] were developed in 2006 using an updated and expanded set of nuclear energy levels. These USD-type Hamiltonians are defined by three single-particle energies (SPE) and 63 two-body matrix elements (TBMEs) in isospin formalism, which are derived from a renormalized G matrix and then fit to a set of binding energies and excitation energies. In this paper, we introduce four new isospin-breaking USD-type Hamiltonians. The spiritual successor, which is based on the same renormalized G matrix *sd*-shell interaction (SDBA) [5], is USDC. Additionally, we derive USDI which uses a new *ab initio* interaction based on a set of in-medium similarity renormalization group (IMSRG) Hamiltonians [6,7] that are nuclei-specific, but otherwise the same fitting procedure is followed. Also presented are USDCm and USDIm in which the Coulomb TBME are further constrained.

The original USD Hamiltonian was obtained from a least-squares fit modified with the singular value decomposition (SVD) method of 380 energy levels with experimental errors of 0.2 MeV or less (with most experimental errors being 10 keV or less) from 66 nuclei with $N \geqslant Z$. The root-mean-square (rms) deviation between experimental and theoretical energies was about 150 keV. USDA and USDB were developed by using the same fitting procedure as USD, with 30 linear combinations of one- and two-body matrix elements varied for USDA and 56 for USDB, with the remaining linear combination fixed values determined by SDBA. The resulting rms deviation between experimental and theoretical energies were 170 and 130 keV for USDA and USDB, respectively. An increased data set was used for USDA and USDB with 608 well-known energy levels in 77 nuclei with $N \geqslant Z$ mainly added data for the middle of the *sd* shell. The distributions of states for these data sets can be seen in Figs. 1 and 2 in Ref. [3]. As these were developed as isospin-conserving Hamiltonians, the energies used in the fit had to be include Coulomb energy corrections [3]. These corrections were obtained from energy differences of isobaric-analog states near the $N = Z$ line.

There exist isospin nonconserving additions to USD consisting of a Coulomb interaction, an isovector term, and an isotensor term [8,9]. These additions were fit to experimental b and c coefficients of the isobaric multiplet mass equation (IMME), without modifying the underlying USD interaction. The addition from Ref. [8] is often used with USDB to perform configuration-interaction calculations and is referred to as USDB-CD. While USDB-CD is quite good at predicting excited energy spectra for *sd*-shell nuclei, it does a poor job at determining absolute ground-state binding energies. Lack of reliable binding-energy calculations results in poor predictions for separation energies.

We are therefore motivated to extend the derivation of USD-type Hamiltonians to include isospin-breaking interactions directly. Isospin formalism restricts the TBME so that the wave functions produced by the interaction have good isospin, thus the inclusion of isospin-breaking terms in the Hamiltonians requires us to move to proton-neutron (pn) formalism. We introduce groupings of TBME to restrict the total number of parameters and keep our results physically

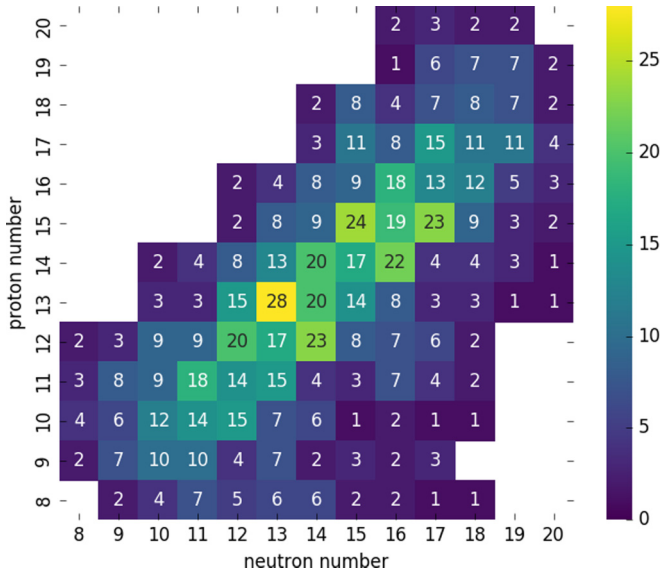

FIG. 1. Number of energy levels in each *sd*-shell nuclei used in the data set for constraining the new Hamiltonians.

reasonable. For the first time, binding energies and excitation energies in proton-rich nuclei are able to be included in the fit and no *a priori* Coulomb corrections to the data are necessary. We are able to consider 854 states in 117 nuclei, and their distribution over *sd*-shell nuclei is shown in Fig. 1. In the Sec. II we discuss the experimental data in more detail. In Sec. III we review the SVD method for the least-squares fit and explain the new additions to the fitting procedure necessary for the charge-dependent terms. In Sec. IV we present the results for the new interactions. Section V covers the modeling of the Thomas-Ehrman shift for specific cases in the *sd* shell that were excluded from the fit. Comparisons of the interactions are done in Sec. VI. Results for separation energies and isospin-level mixing are discussed in Sec. VI.

II. DATA SET

In the last update of the "USD" Hamiltonians in 2006, 608 levels in 77 nuclei were used in $N \geqslant Z$ nuclei in the *sd* shell. This included the 77 ground-state energies and 531 excited-state energies. The distribution of these states in the shell can be seen in Fig. 2 of Ref. [3]. The restriction to neutron-rich nuclei was made because USDA and USDB were made in isospin formalism, which assumed that mirror nuclei were identical apart from a simple Coulomb energy correction. Also for this reason, $T = 1$ isobaric-analog states in the $N = Z$ nuclei were excluded from the data set. These IASs that fit our other criteria described below are included in the updated data set.

By changing our model space to the *pn* formalism, we now allow all well-known *sd*-shell states in nuclei with $8 \leqslant N \leqslant 20$ and $8 \leqslant Z \leqslant 20$, to be used in the data set to constrain our Hamiltonians. This expanded data set includes ground-state energies for 117 nuclei, with at least one excited state included for 107 of those nuclei. Ground-state binding energies used are taken from the 2016 atomic mass evaluation of Wang *et al.* [10] and taken relative to that of ^{16}O,

$$BE(A,Z)^r = BE(A,Z) - BE(^{16}\mathrm{O}). \tag{1}$$

Excited-state energies are taken from the ENSDF database. The number of levels with experimental errors less than 0.2 MeV included in the data set from each nucleus are shown in Fig. 1. Generally, excited states were only included if the J^π for all lower states are known. This is done to ensure that only states with *sd*-shell configurations are included. So-called "intruder states" that involve orbitals outside of our model space are omitted from the data set. These typically occur at high excitation energies where the experimental level density is much higher than the theoretical level density.

Recently, an extensive measurement of the mirror energy differences in ^{27}Al and ^{27}Si was conducted by Lotay [11], providing 43 well-known mirror pairs in the $A = 27$, $T = 1/2$ isobaric pair.

A collection of nuclei with $N = 19,\ 20$ and $Z = 10$–12 are in the "island of inversion" [12]. The ground states of these six nuclei are bound by ≈2 MeV more than expected in *sd*-shell configuration-interaction calculations. This is understood to be due to an inversion of the standard level scheme and requires extension to the *pf* shell to be properly calculated [12]. Ground states and excited states for these nuclei are therefore excluded from the fit.

Several states that have a large Thomas-Ehrman shift (TES) are excluded from the fit. A discussion of these states and analysis of their TES is found in Sec. V.

III. FITTING PROCEDURE AND UNCERTAINTY QUANTIFICATION

The Hamiltonians used in configuration-interaction calculations can be written as a sum of one- and two-body operators:

$$H = \sum_a \epsilon_a \hat{n}_a + \sum_{a\leqslant b,c\leqslant d} \sum_{JT} V_{JT}(ab;cd)\hat{T}_{JT}(ab;cd), \tag{2}$$

where $\hat{n}_a$ is the number operator for the spherical orbit a with quantum numbers (n_a, l_a, j_a) and

$$\hat{T}_{JT}(ab;cd) = \sum_{MT_z} A^\dagger_{JMTT_z}(ab) A_{JMTT_z}(cd), \tag{3}$$

is the scalar two-body density operator for nucleon pairs in the orbits a, b, c, and d coupled to the spin quantum number JM and isospin quantum numbers TT_z.

In this work, we separate the Hamiltonian into three components:

$$H = H_0 + H_{\mathrm{INC}} + H_C, \tag{4}$$

where H_0 is the isospin-conserving strong interaction, H_{INC} is the isospin-breaking portion of the strong interaction, and H_C is the Coulomb interaction. This allows us to separate the eigenvalues λ_k of the full Hamiltonian with eigenvectors ϕ_k into

$$\begin{aligned}\lambda_k &= \langle\phi_k|\, H\, |\phi_k\rangle \\ &= \langle\phi_k|\, H_0\, |\phi_k\rangle + \langle\phi_k|\, H_{\mathrm{INC}}\, |\phi_k\rangle + \langle\phi_k|\, H_C\, |\phi_k\rangle \\ &= \lambda_k^0 + \lambda_k^{\mathrm{INC}} + \lambda_k^C. \end{aligned} \tag{5}$$

The method of fitting used in this work has three levels of sensitivity. First, H_0 was fit by using all available energy levels in the shell, while H_C and $H_{\rm INC}$ are held constant at reasonable initial values. Second, H_C was modified in the case of USDCm and USDIm to reproduce the experimental linear (b) coefficients in the IMME. And lastly, the isotensor strength modification in $H_{\rm INC}$, which is the change in strength for the $T = 1$ pn TBME, was set to minimize the rms deviation of the quadratic (c) coefficients of the IMME. After these steps, we once again fit H_0 while holding H_C and $H_{\rm INC}$ constant at the new constrained values. We explored adding an isovector component to the interactions but found that it could not be well constrained by the data set and did not significantly impact the results of the fits.

As in the derivation of USDA and USDB, a reformulation of the least-squares fit in terms of uncorrelated linear combinations through a SVD of the error matrix is used to constrain the SPE and TBME to experimental energies. The strength of this method is in the separation of well-determined and poorly determined linear combinations, allowing us to replace those not-well-constrained values by using a starting *ab initio* Hamiltonian. A full explanation of this method can be found in Ref. [3].

Briefly, the optimization of the interaction with N_p parameters, $\mathbf{p} = \{p_1, \ldots, p_{N_p}\}$ (the SPE and TBME), that are adjusted to fit N_d experimental energies $E_{\rm exp}$ through the minimization of the chi-squared function:

$$\chi^2(\mathbf{p}) = \sum_{k=1}^{N} \left(\frac{E^k_{\rm expt} - \lambda_k(\mathbf{p})}{\sigma^k} \right)^2, \tag{6}$$

where σ^k are the adopted errors corresponding to the experimental energies and include both experimental and theoretical errors. To minimize the arbitrariness of the selection of the theoretical error, the adopted errors can be tuned so that the chi squared function is normalized to the number of degrees of freedom $N_{\rm dof} = N_d - N_p$ at the minimum $\mathbf{p}_0$.

A new addition to these isospin-breaking USD-type Hamiltonians is a statistical uncertainty for each of the fitting parameters. This was done following the prescription of Ref. [13], first defining the covariance matrix C in terms of the Jacobian J:

$$C \approx (J^T J)^{-1}, \quad J_{i\alpha} = \frac{1}{\sigma^i} \frac{\partial E^k_{\rm expt}}{\partial p_\alpha} \bigg|_{\mathbf{p}_0}. \tag{7}$$

Statistical uncertainties for the fitted parameters can then be calculated as $\Delta p_\alpha = \sqrt{C_{\alpha\alpha}}$. Statistical uncertainties for calculated observables can also be determined using the covariance matrix.

Recently, uncertainty quantification of shell-model parameters in the *sd* shell was carried out by using principal component analysis in Ref. [14].

A. The isospin-conserving interaction

Some changes to the SVD fit method were necessary to transition to the *pn* formalism. It was necessary to group the strong force TBME that would be identical in an isospin-symmetric interaction. For example, the following TBME in isospin formalism transforms into three equal (up to a phase) TBME in *pn* formalism: a proton-proton term, a neutron-neutron term, and a proton-neutron term:

$$\begin{aligned} V_{0,1}(k,k;k,k) \rightarrow\ & V_{0,1}(pk,pk;pk,pk) \\ & V_{0,1}(pk,nk;pk,nk) \\ & V_{0,1}(nk,nk;nk,nk), \end{aligned} \tag{8}$$

where the label k represents an *sd*-shell orbit ($s_{1/2}$, $d_{5/2}$, or $d_{3/2}$) and the prefixes p and n indicate whether it is a proton or neutron orbit, respectively. We therefore want these terms in H_0 to evolve together during the fit. This takes the 202 TBME in H_0 and puts them into 63 TBME groups.

Since we are not fitting the entire Hamiltonian at once, and instead are doing so in stages, we must also subtract the contributions to the energy eigenvalues due to $H_{\rm INC}$ and H_C from the experimental energies in the data set. This is because we wish to minimize the quantity

$$\chi^2 = \sum_{k=1}^{N} \left(\frac{E^k_{\rm expt} - \lambda_k}{\sigma^k_{\rm expt}} \right)^2 = \sum_{k=1}^{N} \left(\frac{\tilde{E}^k_{\rm expt} - \lambda^0_k}{\sigma^k_{\rm expt}} \right)^2, \tag{9}$$

where $E^k_{\rm expt}$ are the experimental energies, $\sigma^k_{\rm expt}$ are the associated errors, and $\tilde{E}^k_{\rm expt} = E^k_{\rm expt} - \lambda^{\rm INC}_k - \lambda^C_k$ is the effective experimental energies used in the first stage of the fit.

B. The Coulomb interaction

Three sources were considered for the two-body Coulomb interaction. The first is an analytic Coulomb potential in the simple harmonic-oscillator basis. A benefit of harmonic-oscillator wave functions is the simplification of the separation into relative and center-of-mass coordinates. Using this potential requires that $\hbar\omega$ have a mass dependence $\approx 41\, A^{-1/3}$ to adequately reproduces the experimental rms charge radii. The consequence of this is an overall mass dependence for the Coulomb TBME of $\langle 1/r \rangle \sim (\hbar\omega)^{1/2} \sim A^{-1/6}$.

We also use a more realistic basis by using a Skyrme energy density functional to calculate a two-body Coulomb interaction. In both cases, corrections to the Coulomb potential to account for short-range correlations and the finite size of the proton can be added. This will be discussed more in Sec. IV. Lastly, we take the Coulomb component of the IMSRG Hamiltonians for nuclei with $N = Z$ in the *sd* shell. The Coulomb contribution to the IMSRG TBME was determined by taking the difference of the pp and nn $T = 1$ terms. We then take an average of these IMSRG Coulomb TBME as another H_C to test in the fit.

The b coefficient of the IMME is due primarily to the Coulomb force. Therefore, the b coefficient rms deviation between experiment and theory calculations is a good test to differentiate these three interactions. In the data set, there are 206 mirror energy states (38 ground-state pairs, and 168 excited-state pairs) with experimental errors <0.2 MeV. It is important to exclude those pairs which have a large Thomas Ehrman shift (TES). Due to different radial extents of the s and d orbitals, the energies of isobaric mirror states are shifted down by the Coulomb interaction [15,16]. These excluded pairs will be discussed in Sec. V.

Just as a SVD fit was done for H_0, the method can be applied to the 30 TBME and 3 SPE in H_C to further reduce the b coefficient rms deviation. This requires reframing the minimization parameter to

$$\chi_b^2 = \sum_{k=1}^{N_b} \left(\frac{b^k_{\rm expt} - b^k_{\rm fit}}{\sigma^k} \right)^2, \tag{10}$$

where

$$b^k = \frac{E^k(T_z = T) - E^k(T_z = -T)}{2T}, \tag{11}$$

for a pair of states in mirror nuclei.

C. The isotensor interaction

Isospin symmetry is not broken solely by the Coulomb interaction, it is also only a partial symmetry for the strong nuclear Hamiltonian. Nucleon-nucleon scattering data have shown that the V_{nn} strength is slightly larger than V_{pp}, and further that V_{np} is greater than the average of V_{nn} and V_{pp}. This has previously been approximated as a 1% increase in the $T = 1$ pn two-body matrix elements and a 1% decrease in the $T = 1$ nn and pp two-body matrix elements. For this work, the same isotensor effect can be captured by simply increasing the $T = 1$ pn matrix elements by

$$V_{J,1}(pn) = (1 + \alpha_T)\left(\frac{V_{J,1}(pp) + V_{J,1}(nn)}{2} \right), \tag{12}$$

with α_T being set initially to 0.02 or 2%. This is also consistent with the results of Ref. [8]. In this work, we also take $V_{pp} = V_{nn}$ in H_0.

While the b coefficient of the IMME is sensitive to the Coulomb interaction, the quadratic (c) coefficient is sensitive to the asymmetry of the pn interaction to the strong components of the nn and pp interactions. Figure 2 shows that the odd-odd to even-even oscillation of the c coefficients for the ground-state $T = 1$ triplets in the sd shell. Introducing Coulomb can only partially explain the size of the oscillation; the addition of an isotensor component creates much better agreement with experiment.

The values of the $V_{J,T=1}(5, 5; 5, 5)$ TBME are -2.5601 MeV ($J = 0$), -0.9894 MeV ($J = 2$), and -0.1982 MeV ($J = 4$) for the strong (isospin-conserving) interaction and 0.4386 MeV ($J = 0$), 0.3852 MeV ($J = 2$), and 0.3612 MeV ($J = 4$). As J increases, there is a much steeper drop-off in the isospin-conserving TBME compared with the Coulomb TBME. And as the isotensor interaction is modeled as proportional to the isospin-conserving TBME, the same drop-off is found in the isotensor TBME.

If there were no J dependence in the TBME, there would be no oscillations in Fig. 2. The weak J dependence in the Coulomb TBME result in small oscillations. It is the strong J dependence in the isotensor interaction that creates the large oscillations in the c coefficients.

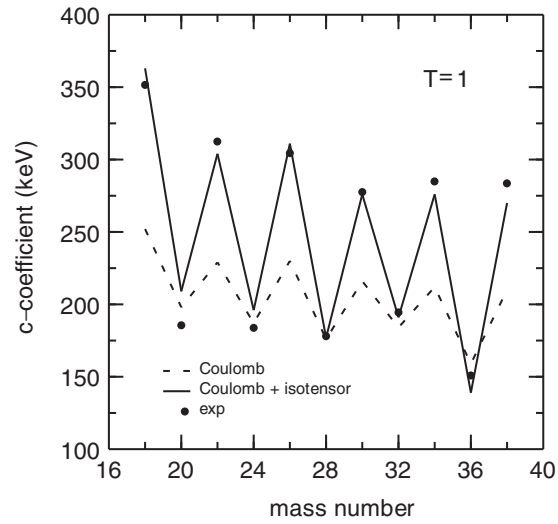

FIG. 2. The c coefficients of the lowest lying $T = 1$ sd-shell triplets. The dashed line shows the contribution to the c coefficients from the Coulomb interaction. The solid line shows the combined contribution from the Coulomb interaction and a 2.2% increase in the $T = 1$ pn two-body matrix elements. Experimental values are shown as filled circles.

IV. RESULTS FOR THE NEW HAMILTONIANS

The calculations for the wave functions and energies were carried out with NuShellX. One iteration for the strong interaction fit took around 2 hours on a multicore desktop PC.

The criteria used to include experimental data in the fit is described in Sec. II. These allow us to consider 854 states in 117 nuclei with errors of less than 0.2 MeV. The uncertainties used in Eq. (6) show the experimental errors $\sigma^k_{\rm expt}$ added in quadrature with a theoretical error set to 0.14 MeV,

$$(\sigma^k)^2 = \left(\sigma^k_{\rm expt}\right)^2 + \left(\sigma^k_{\rm th}\right)^2, \tag{13}$$

in order to normalize the χ^2 to the number of degrees of freedom.

As was done for the previous USD-type Hamiltonians, the SPE are taken to be mass independent. While a mass dependence was explored for the SPE, it does not have a significant effect on the rms deviations because changes in the TBME can compensate.

The TBME have a mass scaling of the form

$$V_{JT}(ab; cd)(A) = \left(\frac{18}{A} \right)^p V_{JT}(ab; cd)\ (A = 18). \tag{14}$$

For the matrix elements in H_0 and $H_{\rm INC}$, we take $p = 0.3$ as described in Ref. [1,3]. The Coulomb TBME scale analytically with $p = 1/6$ as previously shown.

The poorly determined linear combinations of the TBME and SPE were first constrained either with the renormalized G matrix Hamiltonian SDBA, or an average of the $N = Z$ sd-shell IMSRG interactions with the Coulomb matrix elements subtracted out to extract the strong component of the TBME. Using SDBA as the constraining interaction resulted in the USDC Hamiltonian, and replacing SDBA with IMSRG,

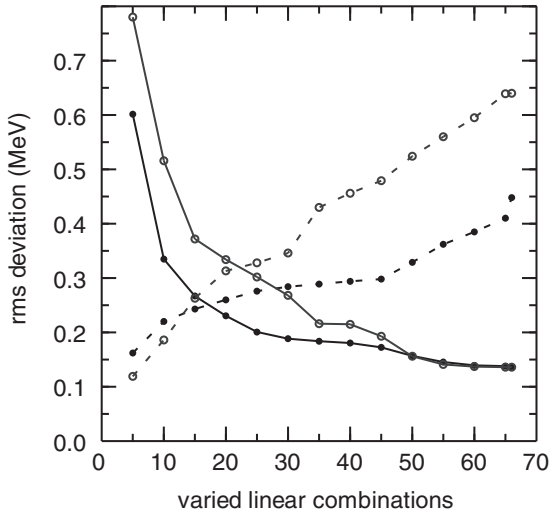

FIG. 3. The rms deviations as a function of the number of fitted linear combinations in the SVD fit for the strong interaction. In black filled circles are the results for USDC, with the blue lines and open circles showing the results for USDI. The solid lines show the energy rms deviation between experimental and theoretical *sd*-shell energies. The dashed lines show the rms deviation between the two-body matrix elements between the resulting Hamiltonians and the *ab initio* interactions that they are based on.

resulted in the USDI Hamiltonian. Variants of USDC and USDI will be discussed later in the paper.

The ISMRG interactions are nucleus dependent. They can have different zero-body terms (the binding energy of the core) and some apparent mass dependence for the SPE. We performed fits allowing a variable zero-body term, and with mass-dependent SPE using the IMSRG for the *ab initio* Hamiltonian. These resulted in either no improvement or a decrease in fit quality. Therefore, we keep a constant zero-body term and SPE for the fits.

In this first stage of the fit there are a total of 69 parameters: the 63 groupings of the isospin-conserving matrix elements, the three SPE due to the strong interaction, and the three SPE due to the Coulomb interaction. The Coulomb TBME were held constant up to the mass scaling, and the isotensor strength was set initially to 2%.

For the first iteration, the USDB matrix elements in *pn* formalism were used for the strong interaction. Starting at $n = 5$ linear combinations being allowed to vary and the remaining poorly determined linear combinations being replaced with the *ab initio* values, we increased n every three iterations until we reached 56 varying linear combinations as used in the derivation of USDB. This was done to allow for slow evolution of the Hamiltonians through parameter space and allow the two different *ab initio* backgrounds to search for different minimums. We then iterated until the Hamiltonian parameters converged to the level of about 10 keV. Results of this SVD fit can be seen in Fig. 3, showing the drop in energy rms deviation as the number of linear combinations allowed to vary is increased, along with an increase in the Hamiltonian rms deviation between the *ab initio* Hamiltonian used and the resulting fitted Hamiltonians.

The rms deviation between experimental and theoretical energies,

$$\text{rms} = \sqrt{\frac{1}{N}\sum_{k=1}^{N}\left(E^k_{\text{expt}} - E^k_{\text{th}}\right)^2}, \tag{15}$$

for USDC and USDI are 139 and 140 keV, respectively. USDC and SDBA have a similar rms deviation between their TBME to that of USDB and SDBA, about 390 keV.

The rms deviation between the USDI and IMSRG TBME is somewhat higher, at 560 keV. Because the IMSRG Hamiltonian is an average of several nuclei-specific IMSRG Hamiltonians, it is not too surprising that the fit diverges more so than it did for SDBA. It is notable that, even though the USDC and USDI were allowed to slowly converge from different starting values, they have a rms deviation for their TBME of 150 keV. The TBME and SPE, and their statistical uncertainties, of these Hamiltonians as well as two others to be discussed can be found in Tables I–III.

We now have two new Hamiltonians based on two different *ab initio* models: USDC from SDBA, and USDI from IMSRG. A visual comparison between the differences of the isospin-conserving TBME in USDC and USDI and the uncertainty of the fit for those parameters are found in Fig. 4. It is clear from the figure that the differences in USDI and USDC are most prominent in the most poorly constrained terms (as expected), and so these terms rely more heavily on the *ab initio* interaction chosen at the beginning. However, we still have the isospin-breaking interactions to consider.

The largest source of isospin symmetry breaking in the nucleus is from the electromagnetic interaction between the protons. We investigated the effects of three distinct sets of Coulomb TBME. The IMSRG Coulomb interaction resulted in a b rms deviation of 72 keV for our set of mirror states. It was found that for the analytic potential, both the Skyrme energy density functional basis and the simple harmonic-oscillator basis resulted in only minor variations of the TBME and produced rms deviations of around 67 keV. Based on these results and to aid in reproducibility, the simple harmonic-oscillator basis was chosen as the source for the two-body Coulomb interaction.

Two corrections to the Coulomb potential were then analyzed to try and improve the b rms deviation. The first is to include the short-range correlations (SRC) of Miller and Spencer [17] through the form factor

$$F_{\text{SRC}}(r) = 1 - e^{-\alpha r^2}(1 - \beta r^2), \tag{16}$$

with $\alpha = 1.1\ \text{fm}^{-2}$ and $\beta = 0.68\ \text{fm}^{-2}$. It should be noted that the IMSRG Coulomb matrix elements include this correction in the renormalization.

The finite size of the proton (FSP) can be accounted for by using the form factor from Wiringa [18],

$$F_{\text{FSP}}(r) = 1 - e^{-x}\left[1 - \left(1 + \tfrac{11}{16}x + \tfrac{3}{16}x^2 + \tfrac{1}{48}x^3\right)\right], \tag{17}$$

with $x = br$, where $b = 4.27\ \text{fm}^{-1}$.

Interestingly, both of these modifications to the underlying analytic potential produce remarkably similar TBME when

TABLE I. Comparison of *ab initio* and fitted isospin-conserving TBME for the *sd* shell in isospin formalism with $T = 1$ (in MeV). Note that $\mathrm{v}(abcd; JT) = V_{JT}(ab; cd)$ ($A = 18$) The orbits are labeled by $1 = s_{1/2}$, $3 = d_{3/2}$, and $5 = d_{5/2}$. The ΔTBME column shows the statistical uncertainties for USDI which are representative for all of our new Hamiltonians.

Matrix element	SDBA	USDB	USDC	USDCm	IMSRG	USDI	USDIm	ΔTBME
v(5 5 5 5; 0 1)	−2.5418	−2.5598	−2.5601	−2.5700	−2.5284	−2.3690	−2.3796	0.0932
v(5 5 3 3; 0 1)	−2.9807	−3.1025	−3.1774	−3.2194	−4.6033	−3.5295	−3.5705	0.1666
v(5 5 1 1; 0 1)	−1.0885	−1.5602	−1.5666	−1.5843	−1.5239	−1.6163	−1.6341	0.0621
v(3 3 3 3; 0 1)	−1.1624	−1.8992	−1.8877	−1.9070	−0.5971	−1.8648	−1.8826	0.0921
v(3 3 1 1; 0 1)	−0.7911	−1.0150	−1.0370	−1.0578	−1.1893	−0.9147	−0.9328	0.0849
v(1 1 1 1; 0 1)	−2.0617	−1.6913	−1.6433	−1.6622	−1.3890	−1.6762	−1.6962	0.0794
v(5 3 5 3; 1 1)	−0.4249	0.6556	0.6030	0.6126	0.6542	0.4130	0.4265	0.1190
v(5 3 3 1; 1 1)	−0.0304	−0.0456	−0.1531	−0.1704	0.1021	−0.2856	−0.3247	0.2107
v(3 1 3 1; 1 1)	0.3994	0.5158	0.5638	0.6042	0.3115	0.6230	0.6655	0.0646
v(5 5 5 5; 2 1)	−0.9932	−1.0007	−0.9894	−1.0151	−0.9087	−0.9777	−1.0076	0.0409
v(5 5 5 3; 2 1)	−0.1394	−0.2137	−0.2289	−0.2254	−0.3810	−0.1917	−0.1924	0.0478
v(5 5 5 1; 2 1)	−0.7957	−0.9317	−0.9274	−0.9579	−0.9790	−0.8992	−0.9241	0.0478
v(5 5 3 3; 2 1)	−0.9399	−1.2187	−1.1421	−1.1623	−1.0623	−1.2787	−1.3037	0.1450
v(5 5 3 1; 2 1)	0.8477	0.8866	0.9137	0.9432	1.0809	0.9979	1.0254	0.0800
v(5 3 5 3; 2 1)	−0.4043	−0.1545	−0.0041	−0.0300	0.4747	0.1943	0.1624	0.1023
v(5 3 5 1; 2 1)	−0.2469	−0.3147	−0.3128	−0.3166	0.1527	−0.3647	−0.3682	0.0603
v(5 3 3 3; 2 1)	−0.9871	−0.5032	−0.7064	−0.7041	−0.7988	−0.8317	−0.8325	0.1020
v(5 3 3 1; 2 1)	0.6449	0.3713	0.4256	0.4292	0.8469	0.3580	0.3515	0.0910
v(5 1 5 1; 2 1)	−1.2335	−0.9405	−0.9690	−0.9939	−0.8554	−0.9738	−1.0042	0.0426
v(5 1 3 3; 2 1)	−0.6317	−0.3173	−0.3807	−0.3791	−0.6018	−0.2549	−0.2519	0.0962
v(5 1 3 1; 2 1)	1.4633	1.6131	1.5668	1.5727	1.4230	1.6142	1.6209	0.0774
v(3 3 3 3; 2 1)	0.1427	−0.0974	−0.0615	−0.0422	−0.1102	−0.0852	−0.0626	0.0282
v(3 3 3 1; 2 1)	0.1787	0.3494	0.3135	0.3247	0.2766	0.3313	0.3427	0.0474
v(3 1 3 1; 2 1)	−0.2767	−0.3034	−0.3338	−0.2940	−0.0167	−0.3463	−0.3048	0.0476
v(5 3 5 3; 3 1)	0.5050	0.7673	0.6476	0.6551	0.2937	0.6708	0.6802	0.0918
v(5 3 5 1; 3 1)	−0.1021	−0.5525	−0.4971	−0.4956	−0.2474	−0.4647	−0.4656	0.0536
v(5 1 5 1; 3 1)	0.2781	0.6841	0.6725	0.6690	0.6042	0.6536	0.6493	0.0536
v(5 5 5 5; 4 1)	0.0356	−0.2069	−0.1982	−0.2087	−0.0631	−0.1906	−0.2032	0.0206
v(5 5 5 3; 4 1)	−1.4942	−1.3349	−1.3256	−1.3133	−1.4737	−1.3335	−1.3215	0.0339
v(5 3 5 3; 4 1)	−1.6941	−1.4447	−1.3904	−1.4069	−0.7751	−1.4937	−1.5106	0.0716

applied separately. When applied together, the TBME decrease noticeably.

With these three options (SRC, FSP, and SRC + FSP) we can once again check the b rms deviations. Each produces a moderate improvement of a few keV to the rms deviation. Given this and for simplicity, we chose to include only the Miller-Spencer short-range correlations to the potential. This Coulomb potential with SRC in the simple harmonic-oscillator basis was used to produce the Coulomb TBME used in USDC and USDI, and will be referred to as Coulomb w/ SRC.

The deviations between experiment and theory for the ground-state and excited-state energies are shown in Fig. 5. Included in the figure are eight points that are not used in the fit. These are the six island-of-inversion ground states and the ground states of ^{27,28}F. The figure shows the results for USDI because at this scale there is no significant difference between USDI and USDC. For each element, the states in neutron-deficient isotopes are to the left in the figure and those states in neutron-rich isotopes are to the right.

The ground states of the six nuclei in the island of inversion (^{29,30}Ne, ^{30,31}Na, and ^{31,32}Mg) that were not included in the fit are under-bound compared with experiment by 1–2 MeV, as shown in the figures. Deviations this large demonstrate the need to expand into the pf model space in order to account for their binding energies [12].

For the new Hamiltonians the neutron-rich fluorine isotopes ($A = 25, 26$) used in the fit show a clear pattern of the theory being overbound when compared with experiment. The ground states of ^{27,28}F are significantly overbound as well, but due to their larger experimental errors of 0.39 MeV they have no impact in the χ^2 minimization. The fit was done with artificially suppressed errors for these fluorine isotopes to see if the Hamiltonian could be forced to reproduce the experimental values without damaging the rest of the fit. The result was that these isotopes could not be forced to these values without harming the fit. The need for further more precise experimental measurements of the neutron-rich fluorine isotopes is clear.

With a Coulomb interaction chosen, we now examine whether further modifying the interaction through a secondary SVD fit can improve our results. States with large TES that are near proton separation energy are excluded from this fit and discussed in Sec. V. A "residual" TES that is present throughout the shell could be accounted for with a modified Coulomb interaction. Such a modification could also be due to

TABLE II. Same as Table I but for the $T = 0$ isospin formalism strong TBME.

Matrix element	SDBA	USDB	USDC	USDCm	IMSRG	USDI	USDIm	ΔTBME
v(5 5 5 5; 1 0)	−1.4315	−1.3796	−1.4302	−1.4317	−1.7115	−1.3929	−1.3981	0.1449
v(5 5 5 3; 1 0)	3.1790	3.4987	3.3480	3.3348	4.8436	3.5507	3.5267	0.1210
v(5 5 3 3; 1 0)	1.7666	1.6647	1.7134	1.7204	1.5594	1.1894	1.2067	0.4152
v(5 5 3 1; 1 0)	0.3628	0.0272	0.2639	0.2854	−0.0049	0.3140	0.3424	0.1734
v(5 5 1 1; 1 0)	−0.8749	−0.5344	−0.5303	−0.5304	−1.0724	−0.3500	−0.3566	0.1734
v(5 3 5 3; 1 0)	−6.5104	−6.0099	−5.9698	−5.9608	−7.4545	−5.6815	−5.6813	0.1595
v(5 3 3 3; 1 0)	−0.0200	−0.1922	−0.2165	−0.2261	0.3890	−0.2293	−0.2489	0.1747
v(5 3 3 1; 1 0)	1.7250	1.6231	1.6755	1.6867	2.8536	1.6872	1.7019	0.1224
v(5 3 1 1; 1 0)	1.8887	2.0226	1.9722	1.9991	2.8861	2.1688	2.1917	0.1049
v(3 3 3 3; 1 0)	−1.3404	−1.6582	−1.6712	−1.6859	−0.0999	−1.5575	−1.5736	0.0947
v(3 3 3 1; 1 0)	−0.8402	−0.8493	−0.6838	−0.6716	−1.2388	−0.7949	−0.7795	0.0893
v(3 3 1 1; 1 0)	0.0405	0.1574	0.1022	0.0821	−0.2347	0.2309	0.2189	0.1387
v(3 1 3 1; 1 0)	−3.3056	−4.0460	−3.8748	−3.9136	−3.7679	−4.0006	−4.0260	0.0912
v(3 1 1 1; 1 0)	−0.2441	−0.9201	−0.9583	−0.9417	−1.0430	−1.0963	−1.0773	0.1054
v(1 1 1 1; 1 0)	−3.3313	−3.7093	−3.6510	−3.6842	−3.0068	−3.5766	−3.6058	0.0944
v(5 3 5 3; 2 0)	−4.5004	−4.2117	−4.2675	−4.2872	−5.1309	−4.5096	−4.5269	0.1454
v(5 3 5 1; 2 0)	−1.2555	−0.6464	−0.7692	−0.7537	−1.6854	−0.8428	−0.8296	0.0986
v(5 3 3 1; 2 0)	−1.4793	−0.4429	−0.2953	−0.2881	−1.6810	−0.3153	−0.3067	0.1317
v(5 1 5 1; 2 0)	−0.4109	−0.3154	−0.3329	−0.3060	−0.4944	−0.3223	−0.2941	0.1331
v(5 1 3 1; 2 0)	−2.7050	−2.5110	−2.4310	−2.4331	−2.6000	−2.2262	−2.2209	0.2112
v(3 1 3 1; 2 0)	−1.3883	−1.8504	−1.9103	−1.9525	−1.6706	−1.8622	−1.9173	0.0860
v(5 5 5 5; 3 0)	−0.8478	−1.6651	−1.5969	−1.5745	−1.2752	−1.6701	−1.6343	0.0766
v(5 5 5 3; 3 0)	2.1769	2.3102	2.2564	2.2574	2.0175	2.1962	2.1934	0.1175
v(5 5 5 1; 3 0)	−1.4992	−1.2167	−1.1785	−1.1770	−2.1032	−1.1734	−1.1821	0.0652
v(5 5 3 3; 3 0)	0.8466	1.1792	1.3317	1.3410	0.2661	1.1406	1.1452	0.1928
v(5 3 5 3; 3 0)	−1.0712	−1.2124	−1.2549	−1.2850	−1.2610	−1.5308	−1.5592	0.1455
v(5 3 5 1; 3 0)	1.0367	1.2526	1.2484	1.2324	1.5017	1.2434	1.2349	0.1455
v(5 3 3 3; 3 0)	2.1625	1.4300	1.1584	1.1576	2.3693	1.2987	1.2928	0.1462
v(5 1 5 1; 3 0)	−3.6000	−4.1823	−4.1134	−4.1194	−3.9772	−4.1631	−4.1546	0.0650
v(5 1 3 3; 3 0)	0.1668	0.0968	0.1126	0.1224	0.0608	−0.1896	−0.1566	0.2127
v(3 3 3 3; 3 0)	−2.9026	−2.9660	−2.9373	−2.9548	−2.8184	−3.0116	−3.0279	0.0444
v(5 3 5 3; 4 0)	−4.4330	−4.6189	−4.5027	−4.4952	−4.5492	−4.0792	−4.0785	0.1536
v(5 5 5 5; 5 0)	−3.6858	−4.3205	−4.3439	−4.3370	−4.0372	−4.3665	−4.3562	0.0342

changes in radii for nuclei in excited sates. Since the Coulomb energy goes as $1/R$, a 1% increase in the radius would reduce the binding energy by about 110 keV. Any model space truncations would also be captured.

The results of the secondary SVD fit can be seen in Fig. 6 showing the rms deviation of the b coefficients and Coulomb Hamiltonian parameters as a function of the number of varied linear combinations. A "modified" Coulomb interaction was chosen by allowing nine linear combinations to vary in the fit. This was motivated by a drop in the b rms deviation and the

TABLE III. Comparison of fitted strong interaction SPE. The orbits are labeled by $1 = 1s_{1/2}$, $3 = 0d_{3/2}$, and $5 = 0d_{5/2}$.

Interaction	ϵ_5	ϵ_3	ϵ_1
USDB	−3.9257	2.1117	−3.2079
USDC	−3.9521(194)	1.8943(1132)	−3.1577(549)
USDCm	−3.8958(189)	1.8887(1134)	−3.1387(538)
USDI	−3.9363(195)	1.8569(1117)	−3.1267(553)
USDIm	−3.8780(190)	1.8517(1117)	−3.1111(541)

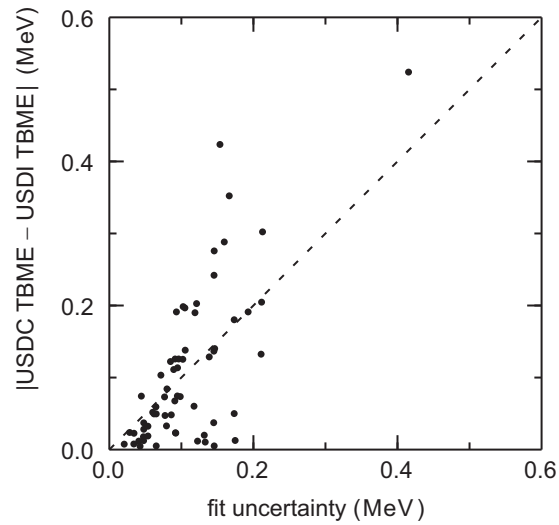

FIG. 4. Absolute differences between the isospin-conserving strong TBME in USDC and USDI plotted against the ΔTBME obtained from the correlation matrix for USDI.

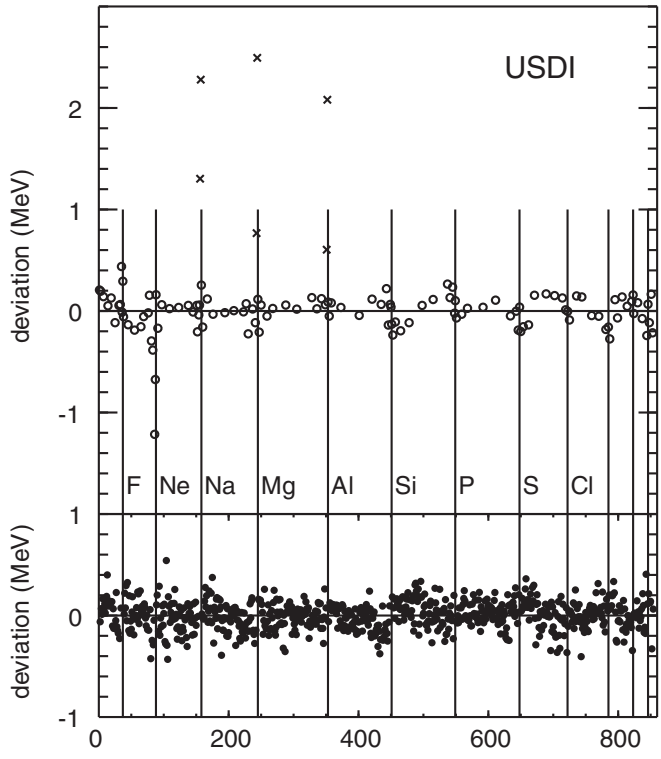

FIG. 5. Deviations between experimental and theoretical energies for USDI. The ground-state binding-energy deviations are plotted on the top, with the excited-state energy deviations plotted on the bottom. The crosses show the deviations for the "island of inversion" nuclei. The fluorine isotopes with large deviations for their ground-state binding energies are discussed in the text.

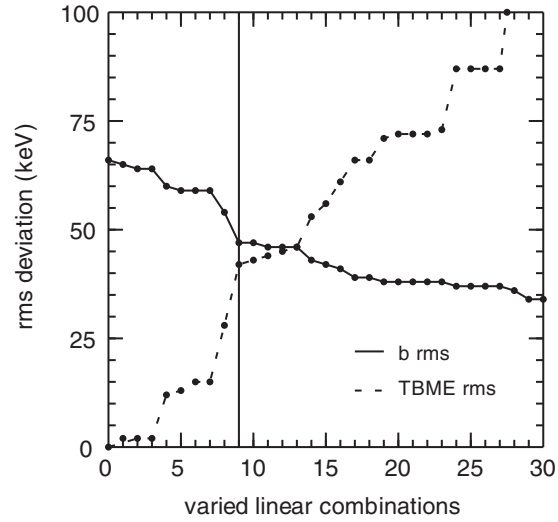

FIG. 6. Results of the SVD fit for the Coulomb interaction. The solid line shows the rms deviation between experiment and theory of the IMME b coefficients. The dashed line shows the interaction rms deviation. The vertical black line at nine varied linear combinations shows our chosen "modified" Coulomb interaction.

first significant change in the TBME and SPE occurring at this point.

The additional data for the $A = 27$, $T = 1/2$ isobaric pair provided by Lotay [11] allows us to compare our modified Coulomb interaction to experiment. It was found that the deviation from experimental b coefficients increased as a function of excitation energy for this mirror pair, with an overall rms deviation of 104 keV. After refitting the Coulomb interaction with these additional data points, this problem was reduced with a new rms deviation for the $A = 27$ data of 48 keV. This improvement can be seen in Fig. 7.

The TBME of this new fitted Coulomb are compared with the Coulomb w/ SRC TBME in Table IV and Fig. 8. Similarly, the SPE are compared in Table V. The fitted Coulomb TBME and SPE are used in USDCm and USDIm. These additional Hamiltonians produce similar plots to Fig. 5 at that scale.

For each of our four new Hamiltonians, we adjusted the isotensor strength increase α_T from 0% to 4% to find the value that produced the lowest c-coefficient rms deviation for 26 isobaric multiplets in the data set. The set of multiplets were composed of 11 triplets ($T = 1$), 10 quartets ($T = 3/2$), and 5 quintets ($T = 2$). All multiplets used involved the ground states of the $|T_Z| = T$ nuclei.

This search determined that the ideal α_T is 2.2% for USDC and USDI which use Coulomb w/ SRC, which agrees well with our initial setting of 2% based on nucleon-nucleon scattering experiments and is consistent with previous theory. For USDCm and USDIm, which use the fitted Coulomb, we find that the minimizing α_T is 0.8%. This lower isotensor strength increase indicates that the fitting of the Coulomb parameters is capturing some of the effects of the isotensor component of the interaction.

Figure 9 shows the theoretical and experimental c coefficients used to constrain α_T. It is clear from the figure that

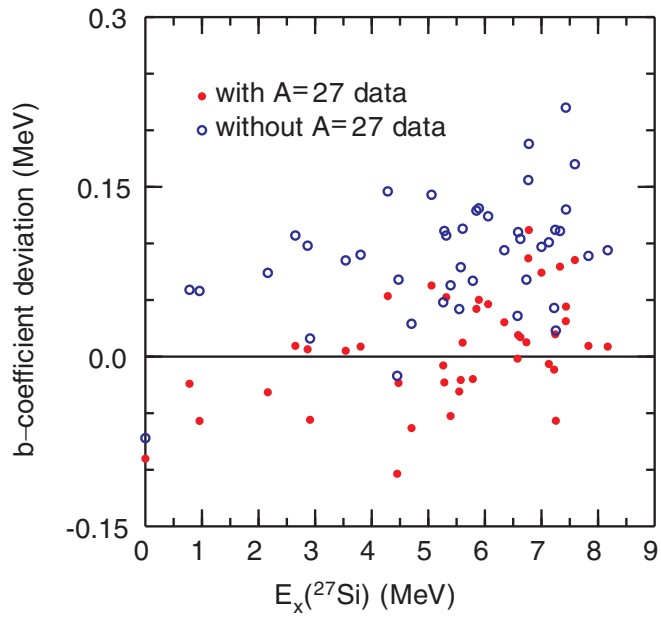

FIG. 7. b-coefficient deviations for the $A = 27$, $T = 1/2$ isobaric pair plotted against the experimental excitation energy of ^{27}Si. The deviation is defined as $\Delta b = b_{\text{expt}} - b_{\text{th}}$.

TABLE IV. Comparison of Coulomb TBME. All orbits are for protons, with $1 = 1s_{1/2}$, $3 = 0d_{3/2}$, and $5 = 0d_{5/2}$.

Matrix element	CD	w/ SRC	Fitted
v(5 5 5 5; 0 1)	0.4386	0.4670	0.4862
v(3 3 3 3; 0 1)	0.4243	0.4525	0.4771
v(1 1 1 1; 0 1)	0.4068	0.4335	0.4477
v(5 3 5 3; 1 1)	0.3958	0.4234	0.4191
v(3 1 3 1; 1 1)	0.3645	0.3901	0.3295
v(5 5 5 5; 2 1)	0.3852	0.4117	0.4556
v(3 3 3 3; 2 1)	0.3615	0.3866	0.3488
v(5 3 5 3; 2 1)	0.3807	0.4071	0.4197
v(5 1 5 1; 2 1)	0.3885	0.4153	0.4838
v(3 1 3 1; 2 1)	0.3805	0.4069	0.3098
v(5 3 5 3; 3 1)	0.3512	0.3758	0.4136
v(5 1 5 1; 3 1)	0.3645	0.3901	0.3909
v(5 5 5 5; 4 1)	0.3612	0.3866	0.3488
v(5 3 5 3; 4 1)	0.3913	0.4178	0.4638
v(5 5 3 3; 0 1)	0.035	0.0355	0.0827
v(5 5 1 1; 0 1)	0.0346	0.0363	0.1010
v(3 3 1 1; 0 1)	0.0283	0.0296	0.1032
v(5 3 3 1; 1 1)	0	0	0.0000
v(5 5 5 3; 2 1)	−0.0112	−0.0123	−0.0107
v(5 5 5 1; 2 1)	0.0238	0.0251	0.1015
v(5 5 3 3; 2 1)	0.0042	0.0041	0.0040
v(5 5 3 1; 2 1)	−0.0194	−0.0205	−0.0233
v(5 3 5 1; 2 1)	0.0168	0.0177	−0.0251
v(5 3 3 3; 2 1)	0.0145	0.0152	0.0047
v(5 3 3 1; 2 1)	−0.0137	−0.0145	−0.0073
v(5 1 3 3; 2 1)	0.0182	0.0192	0.0153
v(5 1 3 1; 2 1)	−0.0196	−0.0205	−0.0233
v(3 3 3 1; 2 1)	−0.0148	−0.0156	−0.0261
v(5 3 5 1; 3 1)	0	0	0.0000
v(5 5 5 3; 4 1)	0.0201	0.0210	−0.0519

USDI better reproduces the c coefficients with a rms deviation of 8 keV compared with the rms deviation for USDIm of 21 keV. Similar results are seen with USDC compared with USDCm.

With the Coulomb and isotensor components of the new Hamiltonians set, we once again fit the isospin-conserving strong interaction. Only one or two iterations were needed for each interaction to converge, and their final values are shown in Tables I–III. Comparisons to the *ab initio* Hamiltonians are shown in Fig. 10.

To recap, the four new interactions developed in this section are

(i) USDC: a constrained G-matrix interaction, an analytic Coulomb term, and a 2.2% increase in the $T = 1$ *pn* matrix elements.
(ii) USDCm: a constrained G-matrix interaction, a constrained Coulomb term, and a 0.8% increase in the $T = 1$ *pn* matrix elements.
(iii) USDI: a constrained IMSRG interaction, an analytic Coulomb term, and a 2.2% increase in the $T = 1$ *pn* matrix elements.

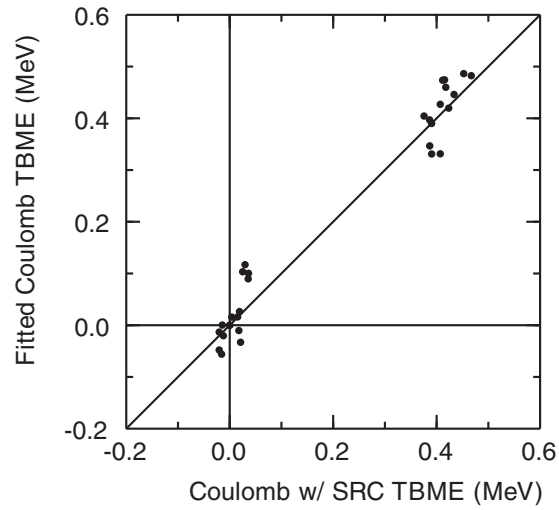

FIG. 8. Comparison of the Coulomb w/ SRC TBME and the fitted Coulomb TBME. The fitted Coulomb was taken as the Coulomb interaction resulting from nine varied linear combinations in Fig. 6. Values for the TBME are shown in Table IV.

(iv) USDIm: a constrained IMSRG interaction, a constrained Coulomb term, and a 0.8% increase in the $T = 1$ *pn* matrix elements.

V. MODELING THE THOMAS-EHRMAN SHIFT

The TES is described as a drop in energy of a state with a valence proton in the $s_{1/2}$ orbit at or near the separation energy due to an increased radial extent of the proton's wave function. The data used in the SVD fit described in Sec. III B had six mirror state pairs removed from the fit due to large TES in their proton-rich nuclei. In this section we will examine these and select other cases with large TES in the *sd* shell.

By using the Skyrme interaction from Ref. [19] with an ^{16}O core, we adjust the depth of the valence $s_{1/2}$ proton orbit while holding the other orbits constant in order to model the single-particle TES. This enables us to calculate the expected TES for any given proton separation energy for the orbit. Doing this at many different separation energies shows that a logarithmic curve fit can be used to predict the TES as a function of proton separation energy. This was then done for a ^{28}Si core and it was found that the single-particle TES curve generated was very similar to the curve of the ^{16}O core. This allows us to use a single curve to model the single-particle TES, of the form

$$\mathrm{TES}_{sp} = -0.4582 + 0.2154\ \ln(S_p + 1.1818), \qquad (18)$$

TABLE V. Comparison of fitted Coulomb interaction SPE. The orbits are labeled by $1 = 1s_{1/2}$, $3 = 0d_{3/2}$, and $5 = 0d_{5/2}$. These are for proton orbits only.

Interaction	ϵ_5	ϵ_3	ϵ_1
CD	3.5749	3.5260	3.4843
w/ SRC	3.6279(137)	3.4514(177)	3.3238(434)
Fitted	3.5122(460)	3.4642(2696)	3.3136(841)

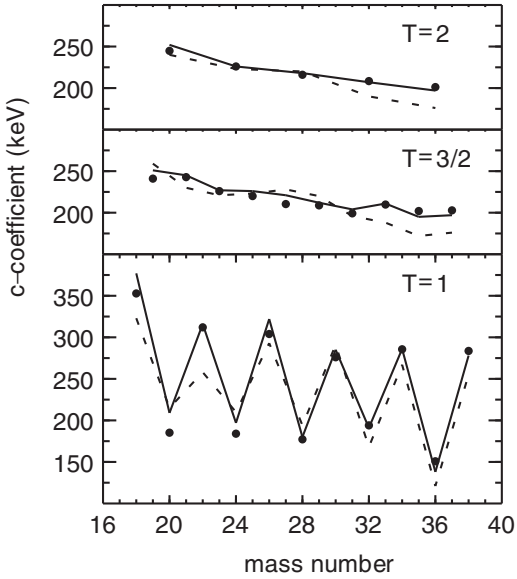

FIG. 9. c coefficients for the lowest lying triplets, quartets, and quintets in the *sd* shell. The solid black line shows the values for USDI, the dashed line for USDIm, and experiment is shown as filled circles.

where TES_{sp} is the single-particle TES in MeV, and S_p is the valence proton separation energy in MeV. This function is plotted in Fig. 11.

In reality, the valence proton is not in a pure $s_{1/2}$ state, and so only a fraction of the state experiences a TES. This fraction corresponds to the spectroscopic factors of the state to the proton $s_{1/2}$ orbit. We can write the total TES for a nucleus ${}^{A}Z$, using the appropriate spectroscopic factors to states in the ${}^{A-1}Z-1$ nucleus, as

$$\mathrm{TE}_{\mathrm{total}} = \sum_{E_x<4\,\mathrm{MeV}} \mathrm{TE}_{\mathrm{sp}}(S'_p)\; C^2S(E_x), \tag{19}$$

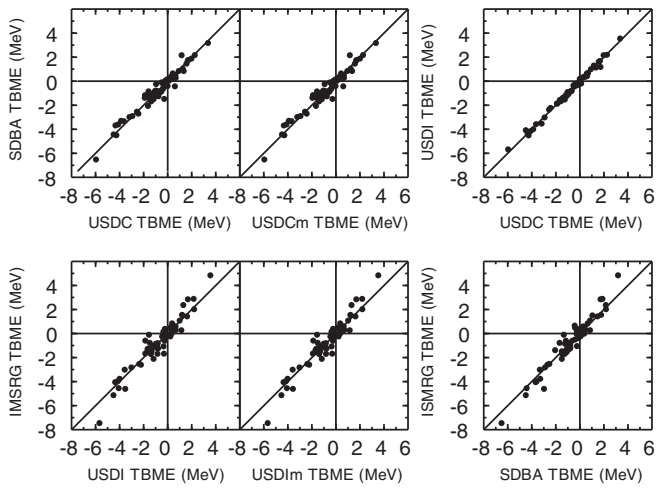

FIG. 10. Comparisons of the fitted and *ab initio* TBME. Only the isospin-conserving TBME in isospin formalism are shown. These are representative of the 63 TBME groups.

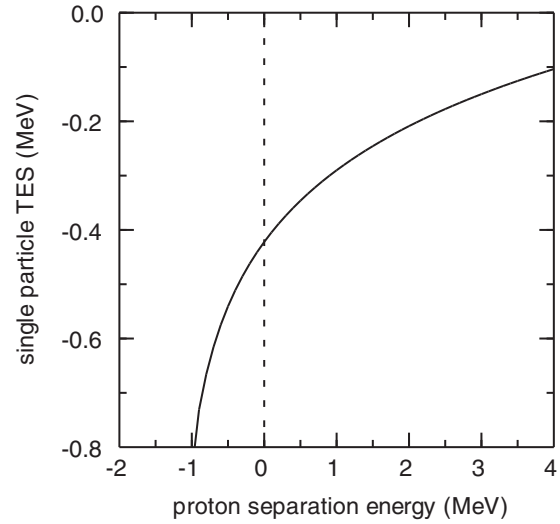

FIG. 11. Thomas-Ehrman shift as a function of proton separation energy, fit to calculations using a Skyrme interaction.

where E_x is the excitation energy of the ${}^{A-1}Z-1$ nucleus, and $S'_p = S_p({}^{A}Z) + E_x({}^{A-1}Z-1) - E_x({}^{A}Z)$.

Table VI shows the analysis of the cases excluded from the b-coefficient SVD fit. The TES of ground states of these nuclei were calculated and found to negligible, and so the shift for the excited levels are all that are shown. The $\mathrm{TE}_{\mathrm{sp}}$ for these cases were taken from the curve in Fig. 11. The 3^+ state in ^{20}Na reported in the table at 2645 keV was originally reported as a 1^+ in Ref. [20], guided by the spin sequence of the mirror nucleus ^{20}F. Indeed, the NNDC database still lists this state as (1^+). It was later argued to be a 3^+ in Refs. [21–23] by process of elimination of possible mirror states.

For each case in the table, the calculated $\mathrm{TE}_{\mathrm{total}}$ is in better agreement with the experimentally measured shift than is the shift calculated using USDC alone. The shift that is built into USDC ranges from 30% to 75% of the calculated $\mathrm{TE}_{\mathrm{total}}$, with the average being about 50%. This can be seen in Fig. 12, where the $\mathrm{TE}_{\mathrm{total}}$ calculation is labeled as Skyrme. Also shown in this figure are the TES built into USDCm, which are similar in magnitude to those in USDC.

This analysis can also be applied to ground states with large $s_{1/2}$ spectroscopic factors; however, we cannot simply add the calculated shift to the mirror energy to compare with experiment.

With USDC, ^{26}P is calculated to have $S_p = -146$ keV. Estimates for the unmeasured S_p for ^{26}P include 140(200) keV [10], 0(90) keV [24], 85(30) keV [25], and $-119(16)$ keV [26]. Using this range of values and the method outlined above, we calculate an expected $\mathrm{TES}_{\mathrm{total}}$ of $-255(14)$ keV. If we assume that USDC again has 30%–75% of the shift built into it, we can revise the separation energy to include the additional shift from this analysis. The predicted USDC + TES one-proton separation energy is then $-12(65)$ keV, the central value of -12 keV corresponding to a proton emission half-life of 7.6×10^{20} years.

We model the one-proton decay as a proton in a single-particle $s_{1/2}$ orbit with a ^{25}Si core, and then calculate the width

TABLE VI. Calculated Thomas-Ehrman shifts for selected nuclei using USDC and the single-particle TES model described in Sec. V. Spectroscopic factors are to the $s_{1/2}$ orbit and calculated with USDC. The C^2S, S'_p, and J_f (spin-parity of the state in the $^{A-1}Z-1$ nucleus) for the dominant term of the sum in Eq. (19) are shown. $E^{\rm expt}_{\rm mirr+TE}$ is the experimental energy for the neutron-rich state in the mirror pair plus the calculated $\rm TE_{total}$.

Nucleus	J^Π	C^2S	J_f^Π	S'_p (keV)	$\rm TE_{sp}$ (keV)	Mirror	$E^{\rm expt}_{\rm mirr}$ (keV)	$E^{\rm expt}_{\rm mirr+TE}$ (keV)	$E^{\rm expt}$ (keV)	$\rm TE_{USDC}$ (keV)	$\rm TE_{total}$ (keV)	$\rm TE_{expt}$ (keV)
^{17}F	$1/2^+$	1.000	0^+	105	−404	^{17}O	870	466	495	−304	−404	−375
^{19}Na	$1/2^+$	0.789	0^+	−1068	−926	^{19}O	1472	741	745(12)	−225	−731	−727(12)
^{20}Na	3^+	0.406	$5/2^+$	−580	−568	^{20}F	2966	2736	2645(2)	−156	−230	−321(6)
	1^+	0.413	$1/2^+$	−811	−672		3448	3168	3001(6)	−122	−281	−447(2)
	0^+	0.559	$1/2^+$	−896	−728		3526	3098	3086(2)	−247	−407	−440(2)
^{23}Al	$1/2^+$	0.704	0^+	−409	−514	^{23}Ne	1017	655	550(20)	−146	−362	−467(20)

of the unbound state at various values of S_p. With this method, we calculate a half-life of 0.046 ms for our most unbound separation energy prediction within uncertainty, $S_p = -77$ keV. A typical beta-decay half-life of 100 ms corresponds to $S_p = 57.5$ keV in this approximation. The beta-decay half-life of ^{26}P has been measured as 43.7(6) ms [24]. We conclude that the lifetime is likely dominated by the β decay,

The proton-dripline can be defined as the point at which adding a proton to a nucleus results in a negative one- or two-proton separation energy. With this definition, our prediction of the ^{26}P one-proton separation energy of −12(65) keV puts the nucleus outside of the dripline (ignoring uncertainty). However, up until a negative S_p of about 100 keV the nucleus is still able to undergo β decay. The point at which proton emission dominates over β decay is another definition of the proton-dripline.

USDC predicts that the one- and two-proton separation energies for ^{26}S to be −217 and −1820 keV, respectively. For ^{30}Ar, it predicts one- and two-proton separation energies of −199 and −2976 keV. These nuclei are then good candidates to consider as two-proton emitters, because a sufficiently large TES could cause them to be bound to one-proton emission while leaving the two-proton channel open. However, the daughter nuclei from one-proton decay (^{29}Cl and ^{25}P) also have ground states with large $s_{1/2}$ spectroscopic factors. This has the effect of keeping the ^{26}S and ^{30}Ar unbound to single proton emission by a few hundred keV.

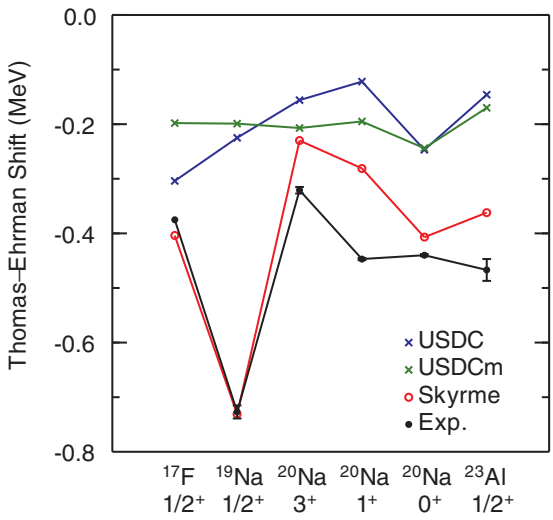

FIG. 12. Comparison of TES found in Table VI.

VI. COMPARING THE NEW HAMILTONIANS

The average, or monopole, interaction energy between two orbits a and b is defined as

$$\bar{V}_{ab,T} = \frac{\sum_J (2J+1) V_{JT}(ab;ab)}{\sum_J (2J+1)}. \tag{20}$$

These monopole interaction energies combine with the SPE to create effective SPE with Z and N dependence. The monopole interactions for our new Hamiltonians are compared in Fig. 13. A similar figure appears in Ref. [3] that is known to show incorrect values. They are split into three groups, the $T = 0$ and $T = 1$ isospin-conserving monopoles, and the Coulomb only $T = 1$ monopoles that involve only

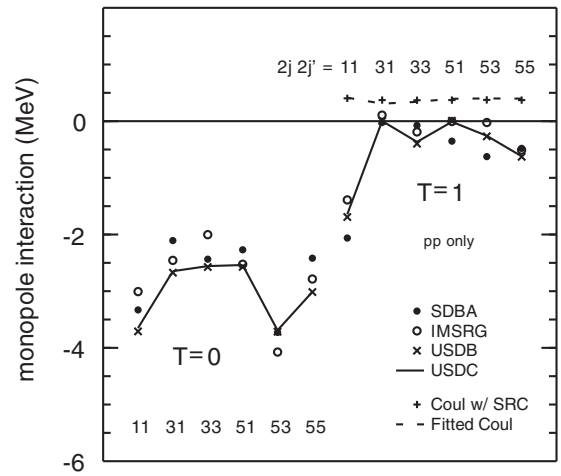

FIG. 13. The *sd*-shell monopole interactions. The solid line show the values for USDC, which are representative of all four new interactions at this scale. The filled circles are for SDBA, the open circles for IMSRG, and the crosses for USDB. The Coulomb monopole interactions are also shown, with Coulomb with SRC as pluses and the fit Coulomb shown as a dashed line. Note that these are for proton-proton matrix elements only.

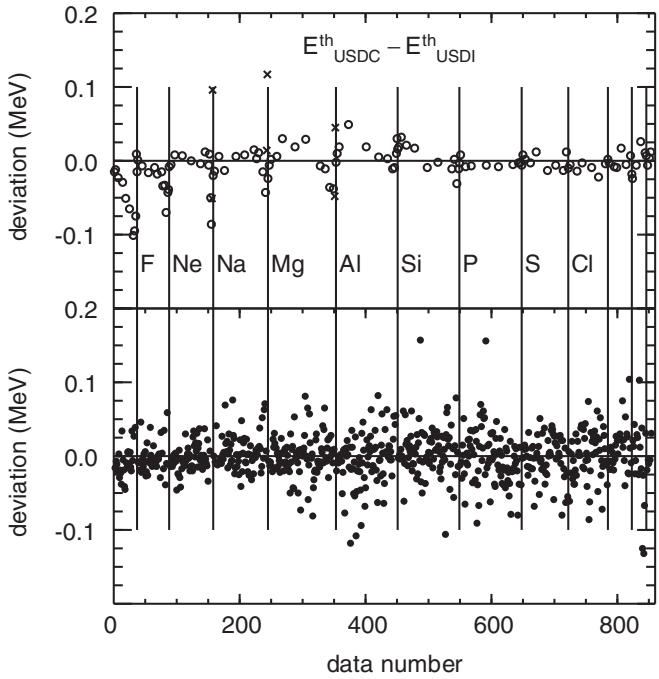

FIG. 14. The deviations of theoretical predictions for ground-state binding energies and excitation energies between USDC and USDI. Excited states are shown in the bottom panel, with ground states in the top.

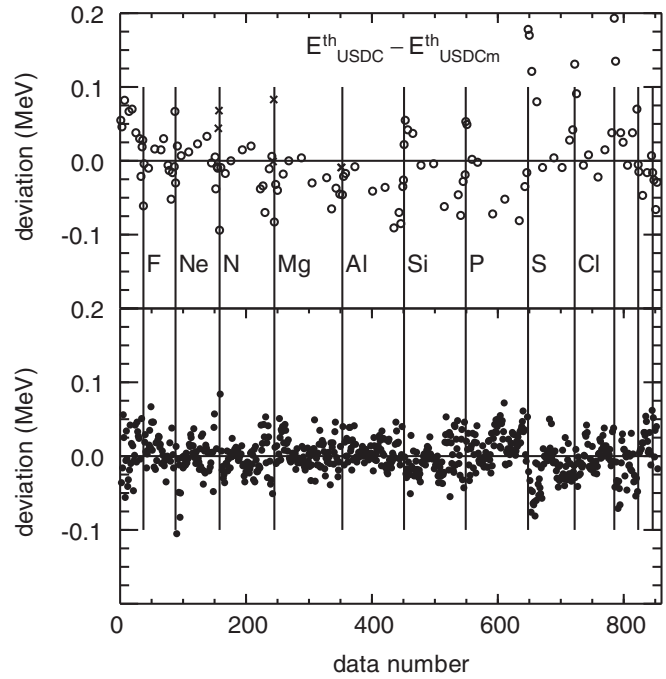

FIG. 15. The deviations of theoretical predictions for ground-state binding energies and excitation energies between USDC and USDCm. Excited states are shown in the bottom panel, with ground states in the top.

pp TBME. The isospin-conserving monopole interactions for USDC, USDCm, USDI, and USDIm are all very similar with the largest deviation being around 100 keV.

The terms with the largest variance among the new Hamiltonians, $d_{5/2} - d_{3/2}, T = 0$ and $s_{1/2} - s_{1/2}, T = 0$, are also the terms that differ from USDB the most. The IMSRG and SDBA monopole strengths differ by up to 600 keV in some cases, but have a similar pattern.

The six $T = 1$ monopole terms for our fitted Coulomb are shown to be in good agreement with the Coulomb w/ SRC, with most being within 5%. The $pd_{3/2} - ps_{1/2}$ term has the largest shift, with a decrease of 64 keV or 17% of the unfitted value.

Looking at the differences between energy-level predictions using our new Hamiltonians can serve to help understand the theoretical uncertainties in those predictions. In Fig. 14 the residuals between USDC and USDI are shown for both the ground states and excited states, having rms deviations of 24 and 70 keV for each group, respectively. The rms deviation for all of the data is 30 keV, but is clear that the spread is larger in the middle of the shell for the excited states. This tells us that the choice of *ab initio* interaction from which we build our Hamiltonians has a larger effect on the excited-state energies than it does on the ground-state binding energies.

We can also examine the effect of modifying the Coulomb interaction and isotensor strength by looking at the residuals between USDC and USDCm in Fig. 15. There is a larger change in calculated ground-state binding energies between these two Hamiltonians, with a rms deviation of 70 keV. The excited-state energy residuals are smaller than those between USDC and USDI with a rms of 24 keV. The rms deviation for all of the data is 30 keV.

VII. RESULTS FOR SEPARATION ENERGIES AND ISOSPIN MIXING

One motivation for the development of isospin-breaking USD-type Hamiltonians comes from the relatively poor predictions for ground-state binding energies with USDB-CD. The residuals when compared with experiment for the *sd*-shell nuclei included in our updated data set are shown in Fig. 16. Theory is underbound at the bottom of the shell and becomes overbound as you move up the shell, causing calculated separation energies to be systematically larger than experiment at the top of the shell. Also present are the large deviations for the neutron-rich fluorine isotopes and island of inversion nuclei discussed earlier for the new Hamiltonians.

The binding-energy residuals for USDC (with similar results for the three other new Hamiltonians) are shown in Fig. 17. The problem of overbinding towards the top of the shell is solved, allowing for better predictions for separation energies. Figure 18 shows the USDC two-proton and two-neutron separation energies for *sd*-shell nuclei with $Z \geqslant 10$ and $N \geqslant 10$, respectively. The patterns for two-proton separation energies along isotopic chains and for two-neutron separation energies along isotonic chains are similar in shape, with a shift up in energy due to the Coulomb interaction.

Single proton and neutron separation energies were also calculated, allowing us to define the proton and neutron driplines. Consistent with experiment, the oxygen isotopes

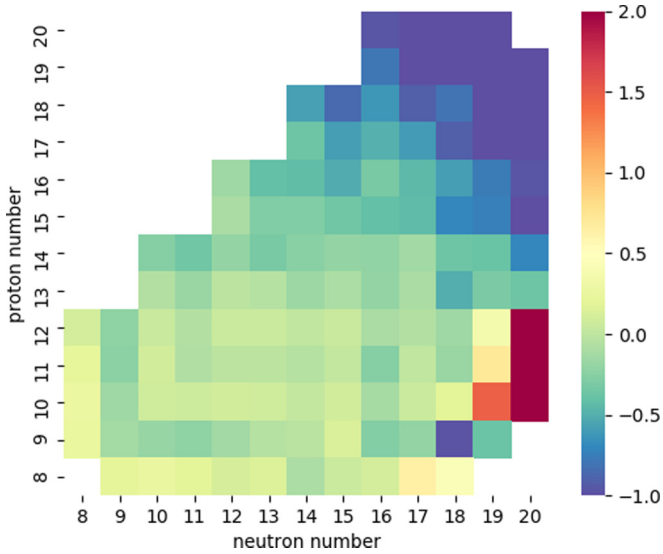

FIG. 16. Differences between the experimental and USDB-CD ground-state binding energies. Positive values indicate that experiment is more bound than theory.

with $A > 24$ are unbound. ^{26,28}O are single neutron bound, but have negative two-neutron separation energies. The only other *sd*-shell nuclei past the neutron dripline is ^{28}F. Figure 19 shows the predictions for the proton dripline and proton separation energies using USDI. For the purposes of this figure, the proton-dripline is defined as the point at which proton-emission dominates the decay. The dripline location is the same for the other new interactions with small changes to the separation energies between them.

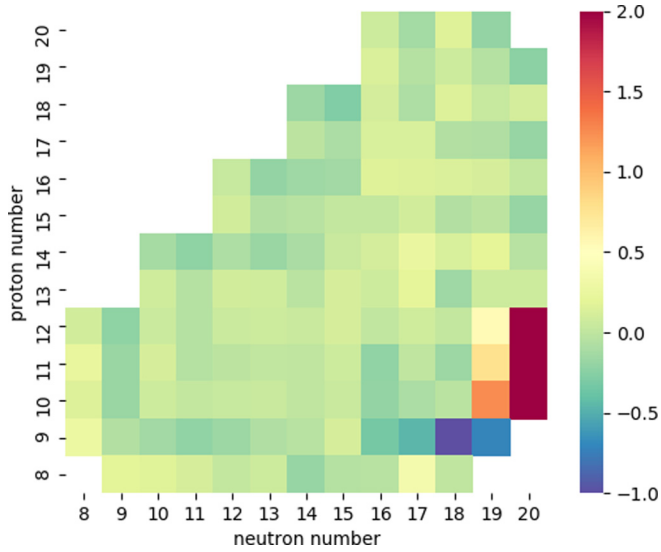

FIG. 17. Differences between the experimental and USDC ground-state binding energies. Positive values indicate that experiment is more bound than theory. There are no significant differences at this scale for calculations using USDI, USDCm, or USDIm. The large disagreement between theory and experiment for the neutron-rich fluorine isotopes is discussed in the text.

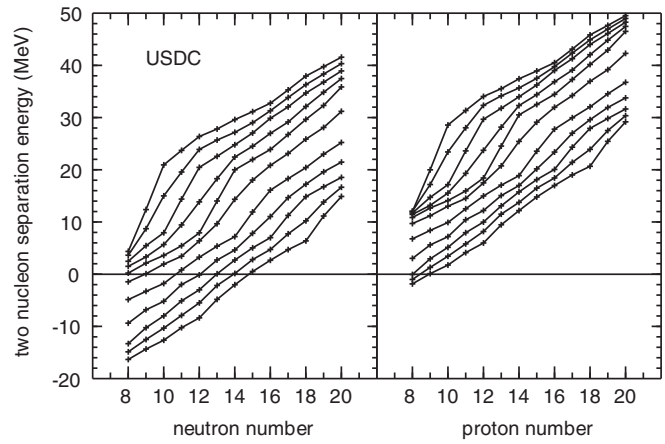

FIG. 18. Isotonic chains of two-proton separation energies (left) and isotopic chains of two-neutron separation energies (right) calculated with USDI. There are no discernible differences at this scale for calculations using USDC, USDCm, or USDIm.

There is only one isotope that is bound to proton emission but unbound to two-proton emission, ^{34}Ca. It has a two-proton separation energy of −2.011 MeV for USDC, −1.991 MeV for USDCm, −2.027 MeV for USDI, and −1.976 MeV for USDIm. These are significantly more negative than the extrapolated mass evaluation value of −1.46(31) MeV [27]. All four Hamiltonians predict that ^{26}P is proton unbound by about 150 keV. However, as discussed in Sec. V, a large TES brings the proton separation energy to −12(65) keV, allowing the nucleus to predominately undergo beta-decay rather than emit a proton.

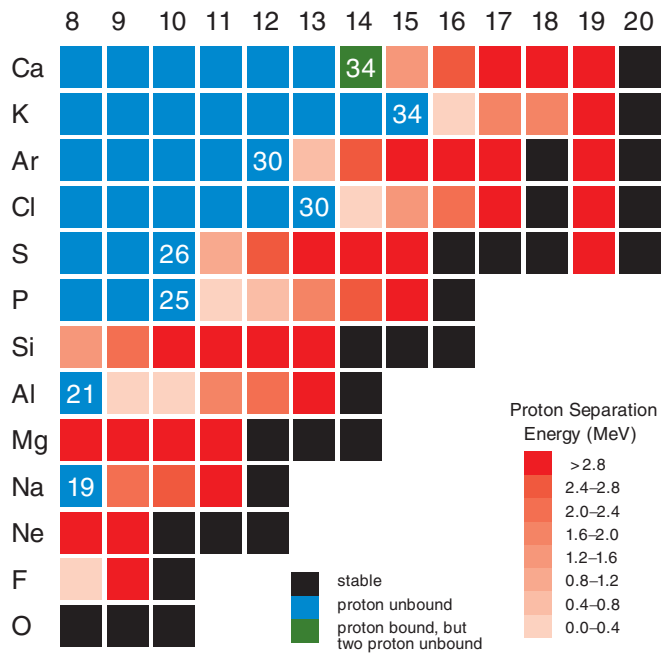

FIG. 19. Predicted proton drip-line and proton separation energies for proton-rich nuclei in the *sd* shell.

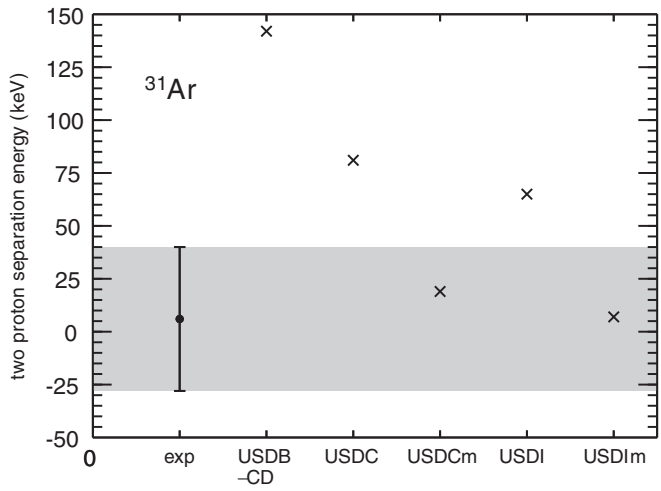

FIG. 20. Experimental and predicted two-proton separation energies for ^{31}Ar.

Recently, the two-proton separation energy for ^{31}Ar was measured as 6(34) keV [28]. Figure 20 shows the theory predictions for USDB-CD and the new interactions compared with this experimental value. The decrease in the separation energy for the new Hamiltonians against USDB-CD is expected, and they are in better agreement with experiment.

A notably large deviation between experiment and theory is found for the proton separation energy of ^{29}Cl. Experiment places the ground state at 1.8(2) MeV above the proton threshold and assigns it as a $1/2^+$ state [29], with an excited $3/2^+$ state at 0.5 MeV. Our configuration-interaction calculations all agree on a ground state at 2.7 MeV above the proton threshold, but with a $3/2^+$ assignment. The first-excited state is then the $1/2^+$ at 0.08 MeV. As mentioned in Sec. V, the $1/2^+$ state has a large proton $s_{1/2}$ spectroscopic factor. A TES of -0.389 MeV is calculated for the $1/2^+$, which causes the inversion of the level scheme as seen in experiment.

With isospin-breaking effective interactions, we can examine isospin-level mixing. Two examples of known large isospin mixing can be found in ^{31}S [30] and ^{32}S [31,32]. The $3/2^+$ levels at 6279 (IAS) and 6390 keV in ^{31}S have a deduced empirical isospin mixing matrix element v of 41(1) keV. Study of the superallowed β transition for ^{32}Cl provided an experimental branching ratio to the 7190 keV state in ^{31}S [32]. Treating this as a two-level mixing problem with the IAS at 7001 keV, as in Ref. [30], the branching ratio was used to deduce $M^2 = 0.0625(42)$. Using our new interactions, we calculate a theoretical B(GT) value of 0.0147(17) (this includes the quenching factor of 0.6). Given that

$$M^2 = \mathrm{B}(F) + \left(\frac{g_A}{g_V}\right)\mathrm{B}(GT), \tag{21}$$

where $(g_A/g_V)^2 = 1.588$, we arrive at a Fermi decay strength of B(F) = 0.039(5). This then translates to an isospin mixing matrix element for the two states of $v = 26(3)$ keV.

TABLE VII. Isospin-mixing matrix elements (keV) between the sixth and eighth $\frac{3}{2}^+$ sd-shell levels in ^{31}S, and the second and third 1^+ sd-shell levels in ^{32}S.

	$v(^{31}\mathrm{S})$	$v(^{32}\mathrm{S})$
Experiment	41(1)	26(3)
USDC	36	23
USDI	38	22
USDCm	51	42
USDIm	56	40
USDB-CD	28	16

Our results are compared with these mixing matrix elements in Table VII. In both cases we see better agreement with experiment for the new USD-type Hamiltonians compared with USDB-CD. Among the new interactions, USDC and USDI and in better agreement with both $v(^{31}S)$ and $v(^{31}S)$ compared with USDCm and USDIm.

VIII. SUMMARY AND CONCLUSIONS

The development of these new "USD" Hamiltonians opens up new avenues to examine isospin mixing and other isospin symmetry-breaking effects in the sd shell. All four new interactions improve predictions for separation energies throughout the shell, eliminating the systematic overestimation present in calculations using USDB-CD.

The calculated binding energies for the neutron-rich fluorine ($N = 16$–19) isotopes are significantly higher than the experimental values found in the 2016 atomic mass evaluation. We suggest further more precise experiments to lower the uncertainties on these measurements, and to correct or reaffirm the current experimental energies.

We have presented four new interactions of two kinds. USDC and USDI use a reasonable Coulomb interaction with no fitting of the Coulomb TBME. USDCm and USDIm have had their Coulomb interaction constrained by a SVD fit to better reproduce the b coefficients of the IMME. An apparent trade-off for this further fitting is a decrease in accuracy for calculating the c coefficients of the IMME. We therefore suggest the use of USDC and USDI for precise predictions of isospin mixing in low-lying states, and USDCm and USDIm for mirror energy differences.

The analytic Coulomb Hamiltonians examined in this paper were still unable to reproduce the energies for several states with large TES. We have shown that individual analysis of these states using a theoretical TES calculated by using a Skyrme interaction can explain the experimental shifts in several nuclei.

ACKNOWLEDGMENT

We acknowledge support from NSF Grant No. PHY-1811855.

[1] B. H. Wildenthal, Prog. Part. Nucl. Phys. **11**, 5 (1984).
[2] B. A. Brown and B. H. Wildenthal, Annu. Rev. Nucl. Part. Sci. **38**, 29 (1988).
[3] B. A. Brown and W. A. Richter, Phys. Rev. C **74**, 034315 (2006).
[4] W. A. Richter, S. Mkhize, and B. A. Brown, Phys. Rev. C **78**, 064302 (2008).
[5] M. Hjorth-Jensen, T. T. Kuo, and E. Osnes, Phys. Rep. **261**, 125 (1995).
[6] S. R. Stroberg, A. Calci, H. Hergert, J. D. Holt, S. K. Bogner, R. Roth, and A. Schwenk, Phys. Rev. Lett. **118**, 032502 (2017).
[7] S. R. Stroberg, H. Hergert, S. K. Bogner, and J. D. Holt, Ann. Rev. Nucl. Part. Sci. **69**, 307 (2019).
[8] W. Ormand and B. Brown, Nucl. Phys. A **491**, 1 (1989).
[9] Y. H. Lam, N. A. Smirnova, and E. Caurier, Phys. Rev. C **87**, 054304 (2013).
[10] M. Wang, G. Audi, F. G. Kondev, W. Huang, S. Naimi, and X. Xu, Chin. Phys. C **41**, 030003 (2017).
[11] G. Lotay (private communication).
[12] E. K. Warburton, J. A. Becker, and B. A. Brown, Phys. Rev. C **41**, 1147 (1990).
[13] J. Dobaczewski, W. Nazarewicz, and P.-G. Reinhard, J. Phys. G **41**, 074001 (2014).
[14] J. M. R. Fox and C. W. Johnson, Phys. Rev. C **101**, 054308 (2020).
[15] R. G. Thomas, Phys. Rev. **88**, 1109 (1952).
[16] J. B. Ehrman, Phys. Rev. **81**, 412 (1951).
[17] G. A. Miller and J. E. Spencer, Ann. Phys. (NY) **100**, 562 (1976).
[18] R. B. Wiringa, V. G. J. Stoks, and R. Schiavilla, Phys. Rev. C **51**, 38 (1995).
[19] B. A. Brown, W. A. Richter, and R. Lindsay, Phys. Lett. B **483**, 49 (2000).
[20] L. O. Lamm, C. P. Browne, J. Görres, S. M. Graff, M. Wiescher, A. A. Rollefson, and B. A. Brown, Nucl. Phys. A **510**, 503 (1990).
[21] N. M. Clarke, S. Roman, C. N. Pinder, and P. R. Hayes, J. Phys. G: Nucl. Part. Phys. **19**, 1411 (1993).
[22] B. A. Brown, A. E. Champagne, H. T. Fortune, and R. Sherr, Phys. Rev. C **48**, 1456 (1993).
[23] D. Seweryniak, P. Woods, B. Blank, M. Carpenter, T. Davinson, S. Freeman, J. Görres, A. Heinz, R. Janssens, H. Mahmud, T. Khoo, Z. Liu, G. Mukherjee, E. Rehm, F. Sarazin, J. Shergur, M. Shawcross, S. Sinha, and A. Woehr, Phys. Lett. B **590**, 170 (2004).
[24] J.-C. Thomas, L. Achouri, J. Äystö, R. Béraud, B. Blank, G. Canchel, S. Czajkowski, P. Dendooven, A. Ensallem, J. Giovinazzo, N. Guillet, J. Honkanen, A. Jokinen, A. Laird, M. Lewitowicz, C. Longour, F. de Oliveira Santos, K. Peräjärvi, and M. Stanoiu, Eur. Phys. J. A **21**, 419 (2004).
[25] H. T. Fortune, Phys. Rev. C **96**, 054329 (2017).
[26] J. Tian, N. Wang, C. Li, and J. Li, Phys. Rev. C **87**, 014313 (2013).
[27] G. Audi, F. G. Kondev, M. Wang, W. Huang, and S. Naimi, Chin. Phys. C **41**, 030001 (2017).
[28] I. Mukha, L. V. Grigorenko, D. Kostyleva, L. Acosta, E. Casarejos, A. A. Ciemny, W. Dominik, J. A. Dueñas, V. Dunin, J. M. Espino, A. Estradé, F. Farinon, A. Fomichev, H. Geissel, A. Gorshkov, Z. Janas, G. Kamiński, O. Kiselev, R. Knöbel, S. Krupko *et al.*, Phys. Rev. C **98**, 064308 (2018).
[29] I. Mukha, L. V. Grigorenko, X. Xu, L. Acosta, E. Casarejos, A. A. Ciemny, W. Dominik, J. Duénas-Díaz, V. Dunin, J. M. Espino, A. Estradé, F. Farinon, A. Fomichev, H. Geissel, T. A. Golubkova, A. Gorshkov, Z. Janas, G. Kamiński, O. Kiselev, R. Knöbel, S. Krupko *et al.*, Phys. Rev. Lett. **115**, 202501 (2015).
[30] M. B. Bennett, C. Wrede, B. A. Brown, S. N. Liddick, D. Pérez-Loureiro, D. W. Bardayan, A. A. Chen, K. A. Chipps, C. Fry, B. E. Glassman, C. Langer, N. R. Larson, E. I. McNeice, Z. Meisel, W. Ong, P. D. O'Malley, S. D. Pain, C. J. Prokop, H. Schatz, S. B. Schwartz, S. Suchyta, P. Thompson, M. Walters, and X. Xu, Phys. Rev. Lett. **116**, 102502 (2016).
[31] D. Melconian, S. Triambak, C. Bordeanu, A. García, J. C. Hardy, V. E. Iacob, N. Nica, H. I. Park, G. Tabacaru, L. Trache, I. S. Towner, R. E. Tribble, and Y. Zhai, Phys. Rev. Lett. **107**, 182301 (2011).
[32] D. Melconian, S. Triambak, C. Bordeanu, A. García, J. C. Hardy, V. E. Iacob, N. Nica, H. I. Park, G. Tabacaru, L. Trache, I. S. Towner, R. E. Tribble, and Y. Zhai, Phys. Rev. C **85**, 025501 (2012).